arXiv:1609.04134v1 [cond-mat.mes-hall] 14 Sep 2016

New scheme for magnetotransport analysis in topological insulators

G. Eguchi* and S. Paschen
Institute of Solid State Physics, Vienna University of Technology, Wiedner Hauptstrasse 8-10, 1040 Vienna, Austria
(Dated: September 15, 2016)

The recent excitement about Dirac fermion systems has renewed interest in magnetotransport properties of multi-carrier systems. However, the complexity of their analysis, even in the simplest two-carrier case, has hampered a good understanding of the underlying phenomena. Here we propose a new analysis scheme that strongly reduces the numerical uncertainty of previous studies and therefore allows to draw robust conclusions. This is demonstrated explicitly for the example of three-dimensional topological insulators. Their temperature and gate voltage-dependent Hall coefficient and transverse magnetoresistance behavior, including the phenomenon of huge linear transverse magnetoresistance, is fully reproduced by the scheme, allowing for an unambiguous identification of the carrier numbers and mobilities. Also the Fermi level can be determined from the analysis. We derive an upper limit for the transverse magnetoresistance as functions of mobility and field. Violation of this limit is a strong indication for field-dependences in the electronic band structure or scattering processes, that are not captured by our model, or for more than two effective carrier types. Remarkably, none of the three-dimensional topological insulators with particularly large transverse magnetoresistance violate the limit.

Keywords: Dirac fermion systems, topological insulators, Hall effect, magnetoresistance

Topological insulators continue to be of tremendous interest to condensed matter physicists [1–3], both to advance the fundamental understanding of topological matter and to pave the way for new applications. Topologically protected states with linear band dispersion have been observed for numerous systems, including $(Bi,Sb)_2(Se,Te)_3$, $TlBi(Se,Te)_2$, Cd_3As_2, and (Ta,Nb)(As,P), by angle-resolved photoemission spectroscopy (ARPES) [4–8]. However, (magneto)transport evidence for electrical conduction by Dirac fermions – relativistic quasiparticle in the solid associated with these bands – has remained more circumstantial [9–13]. This is largely due to finite conductivity contributions from topologically trivial (e.g., bulk) bands. To disentangle the different effects, transport experiments are usually being analyzed with two-carrier models [10, 13–16]. Because of the large number of open parameters in these models, however, this has frequently lead to large uncertainties in the extracted information. As a consequence, unequivocal transport evidence for the expected ultrahigh mobilities of Dirac particles, a cornerstone for "topotronic" devices, remains to be found.

Here we propose a new scheme for such analyses, that largely eliminates previous problems. It clarifies the physical meaning of both the R_H sign inversion and the huge linear transverse magnetoresistance (TrMR) [12, 13], phenomena deemed characteristic of Dirac fermion systems. It also allows to determine the Fermi level as well as the upper limit for TrMR as functions of the Hall mobility and field.

We start by describing the differences between the common two-carrier analysis and our new scheme. In the former, the resistance $R_{xx}(B)$ and the Hall resistance $R_{xy}(B)$, where B is the magnetic field, are characterized by four free parameters (the charge carrier numbers n_1 and n_2, and the mobilities μ_1 and μ_2) and two constant parameters (the charge carrier types q_1, $q_2 = \pm e$, where e is the elementary charge) that need to be anticipated. Following the usual notation, n_i is positive for both electrons and holes, whereas μ_i is negative for electrons and positive for holes. In the new scheme, only two free parameters are used, namely the relative charge carrier number difference

$$N \equiv \frac{n_1 - n_2}{n_1 + n_2} \tag{1}$$

and the relative mobility difference

$$M \equiv \frac{\mu_1 - \mu_2}{\mu_1 + \mu_2} \quad . \tag{2}$$

Two further parameters, the effective Hall coefficient

$$R_H \equiv \lim_{B \to 0} \frac{R_{xy}}{B} \tag{3}$$

and the effective Hall mobility

$$\mu_H \equiv \lim_{B \to 0} \frac{R_{xy}}{R_{xx} B} \tag{4}$$

can be directly read off the data. No *ad hoc* assumption has to be made on the charge carrier type. N and M can thus be determined with minimal ambiguity. q_1 and q_2 are determined as functions of N, M, and μ_H (see supplemental material for the complete description).

Next we show how to understand the sign inversion in R_H, observed in many Dirac fermion systems as a function of temperature T or gate voltage V_G [12, 13]. Figure 1 (a, left) depicts the typically observed signature in consecutive (1-4) $R_{xy}(B)$ traces: the slope varies continuously from 1 to 4. This is to be contrasted with the expectation for $R_{xy}(B)$ traces resulting from a single Dirac

* eguchi@ifp.tuwien.ac.at

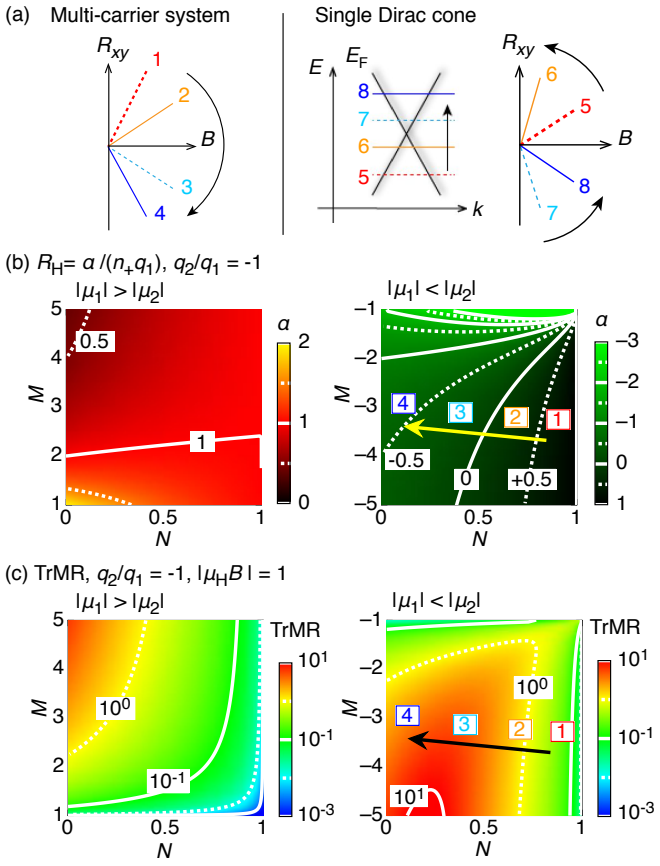

FIG. 1. (Color online) (a, left) Sign inversion of $R_{xy}(B)$ traces typically observed in a multi-carrier system as a function of temperature T or gate voltage V_G (1-4). The slope of $R_{xy}(B)$ varies continuously from 1 to 4. (a, right) Electronic band dispersion of a single Dirac cone, where E is the energy and k is the wave number (left), and corresponding $R_{xy}(B)$ traces at $T = 0$ (right) as E_F is varied across the Dirac point (5-8). The sign change of R_{xy} is accompanied by a discontinuity in the slope of $R_{xy}(B)$. (b) Contour plots of the Hall factor α for $q_2/q_1 = -1$ as functions of N and M, for $|\mu_1| > |\mu_2|$ (left) and $|\mu_1| < |\mu_2|$ (right). The R_H sign inversion occurs only for $|\mu_1| < |\mu_2|$, the situation of higher mobility minority carriers. The four situations (1-4) depicted in (a) could arise, for instance, along the arrow, with sign inversion between 2 and 3. (c) Contour plots of the transverse magnetoresistance TrMR for $q_2/q_1 = -1$ and $|\mu_H B| = 1$ as functions of N and M, for $|\mu_1| > |\mu_2|$ (left) and $|\mu_1| < |\mu_2|$ (right). The same arrow depicted in (c) indicates a monotonic increase between 2 and 3. The upper limits for the TrMR are 5.96 and 12.5 for $|\mu_1| > |\mu_2|$ and $|\mu_1| < |\mu_2|$, respectively.

cone as the Fermi level E_F is varied across the Dirac point (5-8 in Fig. 1 (a, right)) at zero temperature ($T = 0$) [17]. In this case the sign change of R_{xy} is accompanied by a discontinuity in the slope of $R_{xy}(B)$.

If n_1, μ_1, and q_1 denote the majority carrier type ($n_1 > n_2$) and if charge carriers of opposite sign, i.e., both electrons and holes, are present ($q_2/q_1 = -1$), R_H can be expressed as

$$R_H = \frac{1}{n_+ q_1}\alpha \quad , \tag{5}$$

where

$$n_+ = n_1 + n_2 \tag{6}$$

is the total charge carrier number and

$$\alpha = \frac{N + 2M + NM^2}{(N+M)^2} \tag{7}$$

is the Hall factor. The values of the parameters N and M can assume in this case follow from their definitions (Eqns. 1 and 2) as $0 < N < 1$ and $1 < |M| < \infty$. For any (N, M) combination within these limits α directly follows from Eqn. 7. Figure 1 (b) shows contour plots of α in the full N range and for $1 < M < 5$ (left) and $-5 < M < -1$ (right). These describe the situations $|\mu_1| > 1.5|\mu_2|$ and $|\mu_1| < 0.667|\mu_2|$, respectively. Smaller mobility differences would be captured by plots to larger values of $|M|$. These are, however, less relevant here because we aim at separating contributions of highly mobile Dirac fermions from those of topologically trivial fermions with much lower mobility.

Our first key result follows directly from these contour plots. A sign change of α occurs only in the right panel. Therefore, within the two-carrier picture, also R_H can show sign inversion only for $|\mu_1| < |\mu_2|$. In experiments on putative three-dimensional topological insulators (3D-TIs) where the observed sign inversion in R_H was taken as evidence for the presence of Dirac surface states [10, 12, 14, 15], Dirac fermions were thus the minority carriers, and transport was dominated by topologically trivial charge carriers of lower mobility, most likely associated with residual bulk states. To illustrate this further, two concrete examples of temperature and gate voltage tuning are given in what follows.

The experimentally observed R_H sign inversion as a function of temperature can be understood by taking the temperature dependence of the Fermi distribution function $f(E, T)$ into account. Figure 2 (a) shows a sketch of the electronic band structure of a 3D-TI, for the situation where E_F lies above the Dirac point. The Dirac fermions are thus electron like (n-type carriers). The temperature dependence of $f(E, T)$ is also sketched, for different temperatures decreasing from 1 to 4. At high temperatures (1), the majority carriers (n_1) are thermally excited bulk holes (p-type carriers). With decreasing temperature ($1 \rightarrow 4$), n_1 decreases exponentially, resulting in a decrease of n_+ and N. Minor variations are also expected for n_2, μ_1, and μ_2, but they are neglected here for simplicity. To extract information on the system at the sign inversion of R_H, we replot a section of the $\alpha(N, M)$ contour plot of Fig. 1 (b, right) around $|\mu_2/\mu_1| = 5$ ($M = -1.5$), a situation considered realistic for experimentally studied 3D-TIs, in Fig. 2 (b). Upon lowering the temperature

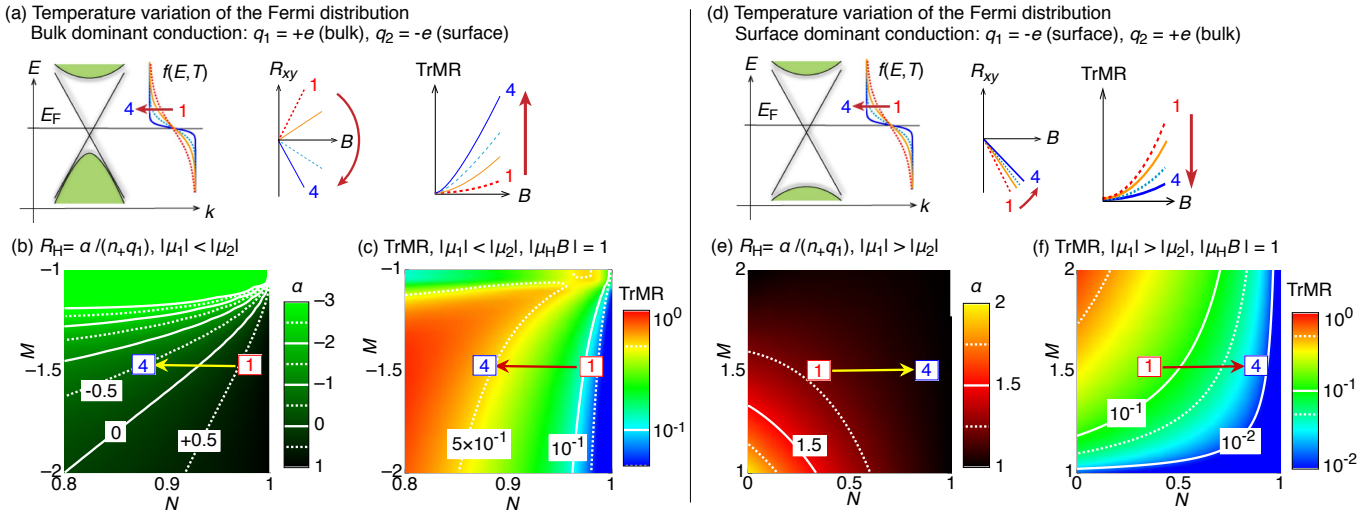
(a) Temperature variation of the Fermi distribution
Bulk dominant conduction: q_1 = +e (bulk), q_2 = -e (surface)
(d) Temperature variation of the Fermi distribution
Surface dominant conduction: q_1 = -e (surface), q_2 = +e (bulk)
(b) R_H= α /(n+q1), |μ1| < |μ2|
(c) TrMR, |μ1| < |μ2|, |μHB| = 1
(e) R_H= α /(n+q1), |μ1| > |μ2|
(f) TrMR, |μ1| > |μ2|, |μHB| = 1
TrMR
N
M
α

FIG. 2. (Color online) (a) Sketch of the electronic band dispersion of a 3D-TI with bulk insulating behavior and minority surface electrons. The Fermi distribution function $f(E,T)$ for four different temperatures (1: highest T, 4: lowest T; left) and consecutive $R_{xy}(B)$ (center) and TrMR(B) (right) traces are also depicted. (b) Contour plot of $\alpha(N,M)$ around $|\mu_2/\mu_1| = 5\,(M = -1.5)$ exhibiting sign inversion at $N = 0.923$ ($n_2 = 0.04n_1$) with decreasing temperature. (c) Contour plot of TrMR(N, M) for $|\mu_H B| = 1$ exhibiting a monotonic increase with decreasing temperature. (d) Sketch of the dispersion for the case of majority surface electrons. Again, $f(E,T)$ for four different temperatures (left), and consecutive $R_{xy}(B)$ (center) and TrMR(B) (right) traces are also depicted. (e) Contour plot of $\alpha(N,M)$ around $|\mu_2/\mu_1| = 5\,(M = 1.5)$ exhibiting no sign inversion with decreasing temperature. (f) Contour plot of TrMR(N, M) for $|\mu_H B| = 1$ exhibiting a monotonic decrease with decreasing temperature.

($1 \rightarrow 4$), sign inversion ($\alpha = 0$) occurs at $N = 0.923$, corresponding to only 4% of surface carriers ($n_2 = 0.04n_1$). Larger mobility differences (smaller negative M values, towards top of Fig. 2 (b)) correspond to even smaller fractions of surface carriers.

Gate voltage tuning can be mimicked by a variation of E_F around the Dirac point (Fig. 3 (a, left), E_F increases from 5 to 8). At not too low temperatures, the above situation with minority surface carriers (n_2) is still relevant here because of the very small density of states of Dirac particles near the Dirac point. The corresponding $R_{xy}(B)$ traces (Fig. 3 (a, center)) and $\alpha(N, M)$ contour plots for $q_2/q_1 = 1$ (E_F below Dirac point, 5 and 6 in Fig. 3 (b, left)) and $q_2/q_1 = -1$ (E_F above Dirac point, 7 and 8 in Fig. 3 (b, right)) reveal the situation at $R_{xy}(B)$ sign inversion (details on α for $q_2/q_1 = 1$ are provided in the supplemental material): For the typical mobility ratio $|\mu_2/\mu_1| = 5$ ($M = -0.667$ for $q_2/q_1 = 1$ and $M = -1.5$ for $q_2/q_1 = -1$) also considered above, it occurs at $N = 0.923$, corresponding to 4% of surface carriers, similar to the temperature tuning case.

Interesting conclusions can, however, also be drawn if $R_H(T)$ reveals no sign inversion. Such a situation may arise in a truly bulk-insulating 3D-TI where surface carriers are the majority carriers (n_1). Here, the exponential decrease of the number of minority bulk holes (n_2) with decreasing temperature ($1 \rightarrow 4$) results in only a small decrease of n_+ (Fig. 2 (d, center)) and an increase of the N (Fig. 2 (e), arrow assumes again a mobility ratio $|\mu_1/\mu_2| = 5$ ($M = 1.5$)). Such a minor effect on the $R_{xy}(B)$ isotherms can, on its own, hardly be taken as strong evidence for the detection of Dirac fermions. However, in conjecture with transverse magnetoresistance measurements, strong conclusions can be drawn, as detailed in what follows.

The transverse magnetoresistance TrMR $\equiv [R_{xx}(B) - R_{xx}(0)]/R_{xx}(0)$ of a two-carrier system with $q_2/q_1 = -1$

$$\mathrm{TrMR} = \frac{(N^2-1)M^2(1-M^2)(\mu_H B)^2}{(2M+N+NM^2)^2 + N^2(1-M^2)^2(\mu_H B)^2} \quad (8)$$

depends on the parameters N, M, and μ_H defined in Eqns. 1, 2, and 4. As stated above, μ_H can be directly read off from $R_{xy}(B)$ and $R_{xx}(B)$ data. Then, for a given $\mu_H B$, TrMR follows for each (N, M) from Eqn. 8. Thus, as for α, contour plots of TrMR(N, M) can be determined and analyzed for the different situations of interest (Fig. 1 (c), Fig. 2 (c, f), Fig. 3 (c)).

The sign inversion in $R_H(T)$ in a system with surface minority carriers (Figs. 1 and 2 (a-c)) is, for the exemplary case of $|\mu_H B| = 1$, accompanied by a monotonic increase of TrMR(T) with decreasing temperature, in agreement with recent experiments [18]. By contrast, if surface carriers are the majority carriers (Fig. 2 (d-f)), TrMR(T) should decrease with decreasing temperature. The sign inversion in $R_H(V_G)$ is accompanied by a distinct feature in TrMR: a non-monotonic variation of TrMR(V_G) with a minimum of TrMR at the Dirac point (Fig. 3 (c)). This insight establishes a new tech-

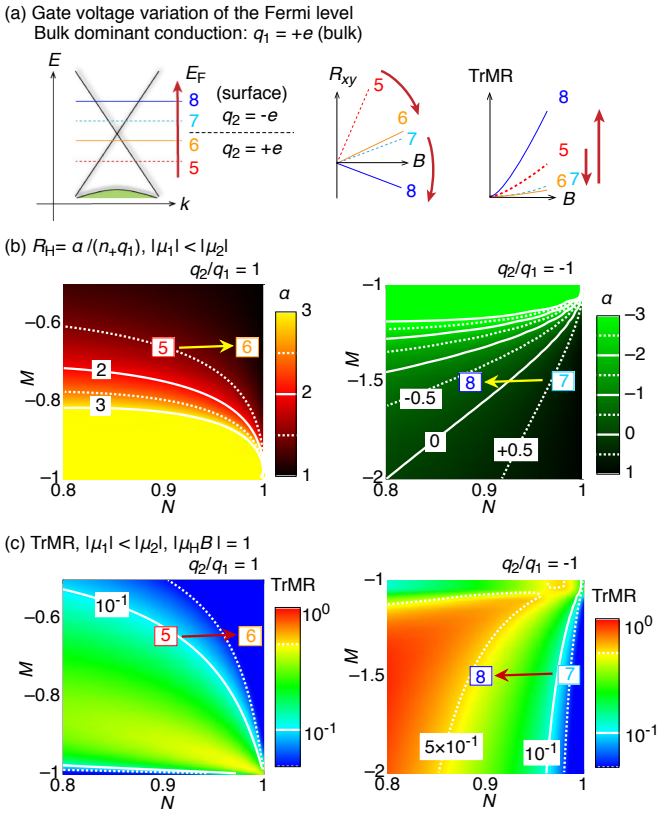

FIG. 3. (Color online) (a) Sketch of the electronic band dispersion of a 3D-TI around the Dirac point. An increase of E_F by V_G (5: lowest E_F, 8: highest E_F; left) and consecutive $R_{xy}(B)$ (center) and TrMR(B) (right) traces are also presented. (b) Contour plots of $\alpha(N, M)$ ($q_2/q_1 = 1$, left) around $|\mu_2/\mu_1| = 5 (M = -0.667)$ and $\alpha(N, M)$ ($q_2/q_1 = -1$, right) around $|\mu_2/\mu_1| = 5 (M = -1.5)$. No sign inversion occurs at the Dirac point ($6 \rightarrow 7$). (c) Contour plot of TrMR(N, M) for $|\mu_H B| = 1$, $q_2/q_1 = 1$ (left) and $q_2/q_1 = -1$ (right). The minimum TrMR is observed at the Dirac point ($6 \rightarrow 7$).

nique to determine the position of the Fermi level [19, 20], complementary to that from Shubnikov-de Haas experiments [10, 14] which are only possible in materials of extremely high quality and/or at very low temperatures. Thus, the simultaneous analysis of both R_{xy} and TrMR within our two-carrier scheme is particularly rewarding and allows to draw robust conclusions.

The phenomenon of TrMR has puzzled researchers since long. A single-carrier Drude model predicts zero TrMR. However, large TrMR values are reported even for the simplest metals such as potassium or copper. This inconsistency was recognized early on [21–23], and was highlighted again more recently in conjecture with the huge linear TrMR observed in Dirac fermion systems [9–13]. Our two-carrier analysis scheme advances the understanding of this phenomenon by revealing that, for any given $|\mu_H B|$ value, there is an upper limit to the TrMR.

Figure 4 shows this TrMR limit for the two cases $q_2/q_1 = \pm 1$ and more mobile minority carriers ($|\mu_1| < |\mu_2|$). Interestingly, the TrMR limit increases linearly with $|\mu_H B|$ for $|\mu_H B| > 10^3$ and $|\mu_H B| > 10^{-1}$ for $q_2/q_1 = -1$ and $q_2/q_1 = 1$, respectively. The corresponding N and M values are also plotted (middle and lower panel). They suggest that linear increase of the TrMR limit with $|\mu_H B|$ occurs if $|\mu_1| \ll |\mu_2|$. The largest TrMR values for various Dirac fermion materials reported in the literature, together with the corresponding μ_H values at the same field, are also summarized in Fig. 4. None of them overshoots the limit. This shows that, surprisingly, all TrMR observed to date are consistent with a two-carrier model.

Let us not conclude without mentioning limitations of our considerations. The two-carrier model assumes that the charge carrier numbers and mobilities, and thus N and M are independent of B. Thus, systems with a strongly B-dependent electronic structure or scattering processes cannot be expected to be described. Whether or not a certain materials class obeys the TrMR limit discussed above is therefore an indication of the validity of these conditions. The fact that a large number of Dirac fermion systems all conform with the TrMR limit (Fig. 4) underpins the validity of this analysis for this materials class. Strongly field-dependent parameters have for instance been observed in strongly correlated electron systems [31, 32], which indeed break the limit [33].

Finally, we mention several possible applications of the new two-carrier analysis scheme. As the two-carrier model does not specify the origin of the carriers, the analysis is valid not only for intrinsic two-band transport, but can also describe extrinsic carriers arising from spatial inhomogeneity or by multi-layer films.

In summary, we have put forward a new two-carrier analysis scheme that clarifies the physical meaning of the R_H sign inversion and the huge linear TrMR. Transport behavior observed in 3D-TIs is discussed. Several features, such as the absence of a sign inversion of R_H in the case where surface carriers are the majority carriers and a minimum of the TrMR at the Dirac point are suggested. Upper limit of the TrMR is determined as a function of $|\mu_H B|$. All huge linear TrMR values observed to date in Dirac fermion systems are consistently explained within the analysis, implying the absence of B-dependent parameters in the two-carrier model.

We acknowledge fruitful discussions with Kenta Kuroda, Akio Kimura, Yuuichiro Ando, and Masashi Shiraishi and financial support from the U.S. Army Research Office (grant W911NF-14-0496) and the Austrian Science Fund (project FWF I2535-N27).

[1] M. Hasan and C. Kane, Rev. Mod. Phys. **82**, 3045 (2010).

[2] X.-L. Qi and S.-C. Zhang, Rev. Mod. Phys. **83**, 1057

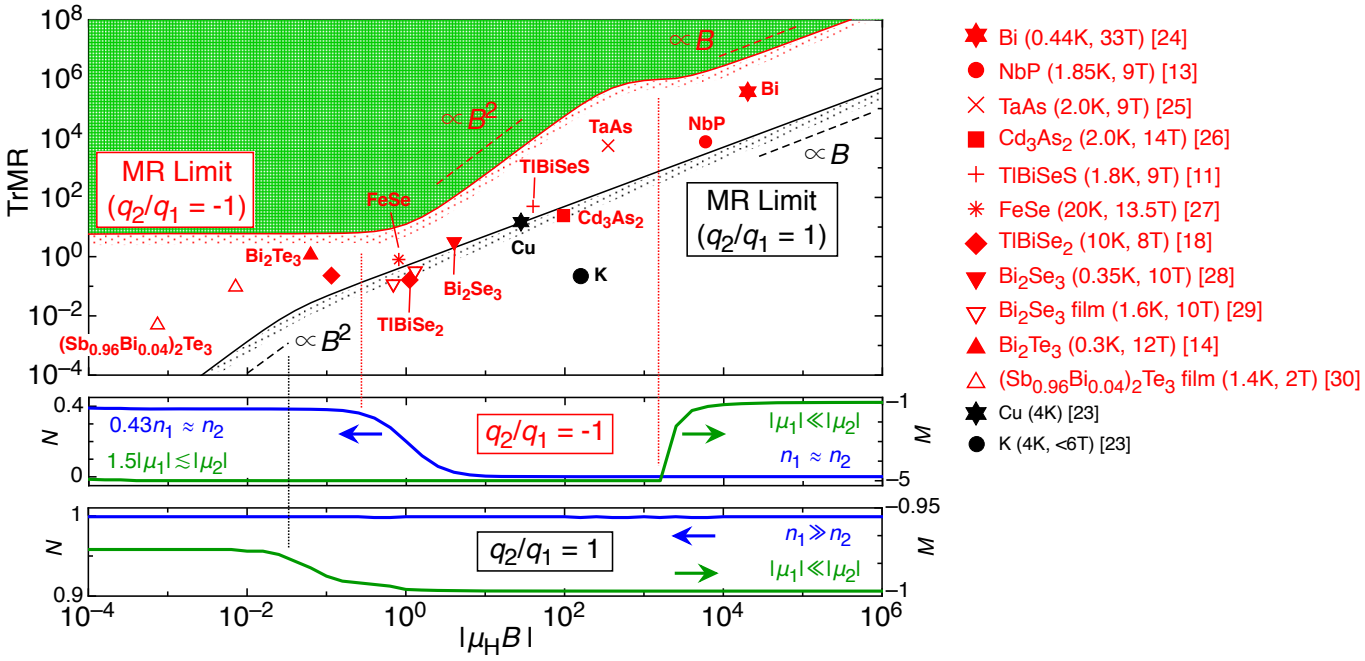

FIG. 4. (Color online) Upper limit of the TrMR for $q_2/q_1 = -1$ (colored in red) and for $q_2/q_1 = 1$ (colored in black) as a function of $|\mu_H B|$. The corresponding N and M values are also plotted. A linear increase of the TrMR limit with $|\mu_H B|$ occurs if $|\mu_1| \ll |\mu_2|$. The largest published TrMR values for various Dirac fermion systems (colored in red) and several pure elements (colored in black) are also plotted [11, 13, 14, 18, 23–30], together with the corresponding $|\mu_H B|$ values given for the same magnetic field in the same reference, for the same sample batch. Remarkably, none of them overshoots the limit.

(2011).
[3] Y. Ando, J. Phys. Soc. Jpn. **82**, 102001 (2013).
[4] H. Zhang, C.-X. Liu, X.-L. Qi, X. Dai, Z. Fang, and S.-C. Zhang, Nat. Phys. **5**, 438 (2009).
[5] K. Kuroda, M. Ye, A. Kimura, S. V. Eremeev, E. E. Krasovskii, E. V. Chulkov, Y. Ueda, K. Miyamoto, T. Okuda, K. Shimada, H. Namatame, and M. Taniguchi, Phys. Rev. Lett. **105**, 146801 (2010).
[6] T. Sato, K. Segawa, H. Guo, K. Sugawara, S. Souma, T. Takahashi, and Y. Ando, Phys. Rev. Lett. **105**, 136802 (2010).
[7] Z. K. Liu, J. Jiang, B. Zhou, Z. J. Wang, Y. Zhang, H. M. Weng, D. Prabhakaran, S.-K. Mo, H. Peng, P. Dudin, T. Kim, M. Hoesch, Z. Fang, X. Dai, Z. X. Shen, D. L. Feng, Z. Hussain, and Y. L. Chen, Nat. Mater. **13**, 677 (2014).
[8] S.-Y. Xu, I. Belopolski, D. S. Sanchez, C. Zhang, G. Chang, C. Guo, G. Bian, Z. Yuan, H. Lu, T.-R. Chang, P. P. Shibayev, M. L. Prokopovych, N. Alidoust, H. Zheng, C.-C. Lee, S.-M. Huang, R. Sankar, F. Chou, C.-H. Hsu, H.-T. Jeng, A. Bansil, T. Neupert, V. N. Strocov, H. Lin, S. Jia, and M. Z. Hasan, Science Advances **1** (2015), 10.1126/sciadv.1501092.
[9] N. P. Butch, K. Kirshenbaum, P. Syers, A. B. Sushkov, G. S. Jenkins, H. D. Drew, and J. Paglione, Phys. Rev. B **81**, 241301 (2010).
[10] Z. Ren, A. A. Taskin, S. Sasaki, K. Segawa, and Y. Ando, Phys. Rev. B **82**, 241306 (2010).
[11] M. Novak, S. Sasaki, K. Segawa, and Y. Ando, Phys. Rev. B **91**, 041203 (2015).
[12] J. Tian, C. Chang, H. Cao, K. He, X. Ma, Q. Xue, and Y. P. Chen, Scientific Reports **4**, 4859 EP (2014).
[13] C. Shekhar, A. K. Nayak, Y. Sun, M. Schmidt, M. Nicklas, I. Leermakers, U. Zeitler, Y. Skourski, J. Wosnitza, Z. Liu, Y. Chen, W. Schnelle, H. Borrmann, Y. Grin, C. Felser, and B. Yan, Nat. Phys. **11**, 645 (2015).
[14] D.-X. Qu, Y. S. Hor, J. Xiong, R. J. Cava, and N. P. Ong, Science **329**, 821 (2010).
[15] F. Yang, A. A. Taskin, S. Sasaki, K. Segawa, Y. Ohno, K. Matsumoto, and Y. Ando, ACS Nano **9**, 4050 (2015).
[16] T. Liang, Q. Gibson, M. N. Ali, M. Liu, R. J. Cava, and N. P. Ong, Nat. Mater. **14**, 280 (2015).
[17] Y. Zhang, Y.-W. Tan, H. L. Stormer, and P. Kim, Nature **438**, 201 (2005).
[18] G. Eguchi, K. Kuroda, K. Shirai, A. Kimura, and M. Shiraishi, Phys. Rev. B **90**, 201307 (2014).
[19] G. Eguchi, K. Kuroda, K. Shirai, Y. Ando, T. Shinjo, A. Kimura, and M. Shiraishi, Phys. Rev. B **91**, 235117 (2015).
[20] H. Emoto, Y. Ando, G. Eguchi, R. Ohshima, E. Shikoh, Y. Fuseya, T. Shinjo, and M. Shiraishi, Phys. Rev. B **93**, 174428 (2016).
[21] N. W. Ashcroft and N. D. Mermin, *Solid State Physics*, 1st ed. (Brooks/Cole, 1976).
[22] C. M. Hurd, *The Hall Effect in Metals and Alloys*, 1st ed. (Plenum Press, New York, 1972).
[23] A. Pippard, *Magnetoresistance in Metals*, 1st ed. (Cambridge University Press, Cambridge, 1989).
[24] K. Behnia, L. Balicas, and Y. Kopelevich, Science **317**, 1729 (2007).
[25] C. Zhang, Z. Yuan, S. Xu, Z. Lin, B. Tong, M. Z. Hasan, J. Wang, C. Zhang, and S. Jia, arXiv:1502.00251 (2015).

[26] J. Feng, Y. Pang, D. Wu, Z. Wang, H. Weng, J. Li, X. Dai, Z. Fang, Y. Shi, and L. Lu, Phys. Rev. B **92**, 081306 (2015).
[27] M. D. Watson, T. Yamashita, S. Kasahara, W. Knafo, M. Nardone, J. Béard, F. Hardy, A. McCollam, A. Narayanan, S. F. Blake, T. Wolf, A. A. Haghighirad, C. Meingast, A. J. Schofield, H. v. Löhneysen, Y. Matsuda, A. I. Coldea, and T. Shibauchi, Phys. Rev. Lett. **115**, 027006 (2015).
[28] B. Fauqué, N. P. Butch, P. Syers, J. Paglione, S. Wiedmann, A. Collaudin, B. Grena, U. Zeitler, and K. Behnia, Phys. Rev. B **87**, 035133 (2013).
[29] A. A. Taskin, S. Sasaki, K. Segawa, and Y. Ando, Phys. Rev. Lett. **109**, 066803 (2012).
[30] J. Tian, C. Chang, H. Cao, K. He, X. Ma, Q. Xue, and Y. P. Chen, Scientific Reports **4**, 4859 EP (2014).
[31] Y. Nakajima, P. Syers, X. Wang, R. Wang, and J. Paglione, Nat. Phys. **12**, 213 (2016).
[32] H. Takatsu, J. J. Ishikawa, S. Yonezawa, H. Yoshino, T. Shishidou, T. Oguchi, K. Murata, and Y. Maeno, Phys. Rev. Lett. **111**, 056601 (2013).
[33] G. Eguchi *et al.*, to be published.